An International Journal of Optimization and Control: Theories & Applications
ISSN: 2146-0957 eISSN: 2146-5703
Vol.16, No.2, pp.428-449 (2026)
https://doi.org/10.36922/IJOCTA025430181

RESEARCH ARTICLE

Optimization of solar chimney performance through CFD modeling and parametric experimental design

Alberto Hananel*, Rodolfo Garcia, and Alejandro Vera

Department of Engineering, Faculty of Engineering, Santo Toribio de Mogrovejo Catholic University, Chiclayo State/Province, Peru
ahananel@ugr.es, rodolfo.garcia@usat.edu.pe, avlazaro@usat.edu.pe

ARTICLE INFO

Article History:
Received: October 21, 2025
Revised: November 20, 2025
Accepted: November 27, 2025
Published Online: January 8, 2026

Keywords:
Computational fluid dynamics (CFD)
Solar chimney power plant
Experimental design
Numerical simulation
Performance optimization
Renewable energy systems

AMS Classification 2010:
76M12; 76R10; 80A20; 76D05; 65N30

ABSTRACT

This study presents a detailed parametric evaluation of solar chimney performance by combining computational fluid dynamics (CFD) simulations with advanced design-of-experiments (DOE) techniques. The analysis focuses on the effects of chimney height, collector-to-chimney AR, chimney geometry, and construction material under realistic environmental conditions. CFD modeling was used to compute airflow, temperature rise, and the resulting buoyancy-driven updraft, while DOE procedures enabled the structured assessment of main effects and interaction effects across geometric factors. The results indicate that larger collector areas relative to chimney cross-section (high AR) and the use of a divergent chimney configuration significantly enhance updraft velocity and mechanical power generation. The configuration with a 30 m chimney and AR = 6 produced an updraft of approximately 12–13 m/s and a power output close to 15 kW, representing the highest performance among all simulated cases. Important interactions between AR and chimney geometry were identified, confirming that single-factor analyses may overlook coupled behaviours relevant to system optimization. These findings offer concise design guidance for enhancing solar chimney performance under local climatic conditions and confirm the feasibility of small, well-optimized systems as a clean-energy option in high-irradiation regions. The analysis is based on steady-state simulations, which inherently simplify real conditions.

1. Introduction

The growing global demand for energy, alongside environmental constraints and the rising costs of fossil fuels, has driven the search for more sustainable renewable sources.[1] In this context, solar energy has emerged as one of the most promising alternatives due to its year-round abundance in many regions.[2] Among solar technologies, the Solar chimney power plant (SCPP) stands out as a feasible option for generating electricity cleanly, with a relatively simple design and minimal environmental impact.[3] An SCPP typically consists of a large-area solar air collector, a central tower or chimney, and turbines at the chimney's base.[4] Ambient air enters beneath the collector and is heated by the greenhouse effect as it absorbs solar radiation, decreasing in density. This hot air naturally rises through the chimney due to buoyancy and drives the turbines to produce electricity (see Figures 1 and 2A for a schematic of the system). Studies report that the turbine conversion efficiency in such systems can reach up to ∼80%

*Corresponding Author

under optimal conditions.[5] Recent experimental surveys have consolidated performance data from multiple SCPP prototypes and climates, providing an updated overview of design options and practical operating ranges.[6]

The first large-scale pilot of a solar chimney was built in Manzanares, Spain, with an output of about 50 kW.[7] Data from the Manzanares plant have served as a benchmark for numerous theoretical and numerical investigations.[8,9] Haaf's early experiments,[8] for example, recorded airflow speeds up to ∼15 m/s in the Manzanares chimney, and subsequent CFD analyses successfully reproduced these magnitudes and the pressure distribution along the tower.[9] Various works have validated CFD models using the Manzanares plant as a base case, confirming that turbulence models of the RNG k-ε type combined with a Discrete ordinates (DO) radiation model can accurately predict the thermal and fluid behaviour of SCPPs.[10] Likewise, experimental studies on smaller-scale prototypes have complemented CFD validation,[11,12] consistently finding highly turbulent flows inside the chimney (Rayleigh numbers on the order of 10^9 or higher).[13] Recent studies also showed good agreement between CFD results and new experimental data,[14] reinforcing the reliability of these modelling tools.

A number of investigations have explored how geometric parameters affect solar chimney efficiency. For instance, the influence of chimney height has been analyzed, demonstrating that taller chimneys increase the updraft (suction) and thus the air flow rate, leading to higher power generation.[15] Similarly, the influence of chimney shape has been widely analyzed. Hu et al.[16] and Xu and Zhou[17] numerically compared a conventional cylindrical tower (Figure 3A) with a divergent solar chimney with a hyperbolic profile (Figure 3B), showing that the divergent configuration can deliver higher power output. Nasraoui et al.[18] reported that a linearly divergent chimney with outlet expansion (Figure 3C) yields slightly lower air velocities than an optimized hyperbolic geometry (Figure 3B). More recent CFD studies on divergent chimneys with modified base-arc and fillet radii have shown additional performance gains for configurations with base expansion (Figure 3(d)).[19] Additionally, parametric analyses indicate that dimensionless groups such as the Grashof number, which characterizes buoyancy forces, correlate directly with power extraction.[20] These findings confirm that chimney and collector geometry exert a major influence on system performance.

Despite the extensive body of numerical and experimental work, most studies have examined one parameter at a time or specific fixed configurations. There is relatively little literature that systematically combines CFD simulation with statistical experimental designs to explore multiple factors simultaneously. Such an approach can provide a more comprehensive view of how different parameters interact. It is worth noting that solar chimney technology is considered scalable: ambitious SCPP projects of 200 MW in Australia and 40 MW in Namibia have been proposed,[21] although their enormous dimensions pose implementation challenges, especially in urban or populated areas.[22,23] Designing these plants optimally requires accounting for local climatic conditions (solar irradiance, ambient temperature, winds), which can be obtained from tools like RETScreen[24] or the Global Solar Atlas.[25] In particular, northern Peru (the Lambayeque region) receives high solar radiation throughout most of the year. This motivated our assessment of the viability of implementing solar chimneys in that locale. Clean energy technologies like SCPPs not only contribute to the energy mix but can also have positive social impacts, helping to meet basic needs in isolated communities (such as providing potable water, drying foods, etc.) Recently, Behera et al.[26] provided an updated review of solar chimney technology and performance, underscoring the continued interest in optimizing these systems.[27] Modern multi-objective optimization algorithms have also been applied to SCPPs, integrating evolutionary techniques with machine learning to improve design efficiency,[28] and techno-economic studies of hybrid solar chimneys equipped with air filtration units have demonstrated how power generation and auxiliary environmental services can be optimized simultaneously.[29]

In this work, we propose an interdisciplinary approach to optimise the performance of solar chimneys, integrating CFD simulation with statistical experimental design methods. The main objective is to identify the combinations of design factors (geometric and environmental) that maximize the power output of the solar chimney, thereby providing design guidelines for future projects in high-irradiation regions such as Lambayeque. To frame the optimization problem, a simplified theoretical analysis was first developed to understand how key geometric ratios influence the flow–highlighting that greater chimney height amplifies buoyant draft, a divergent chimney increases the driving pressure difference, and

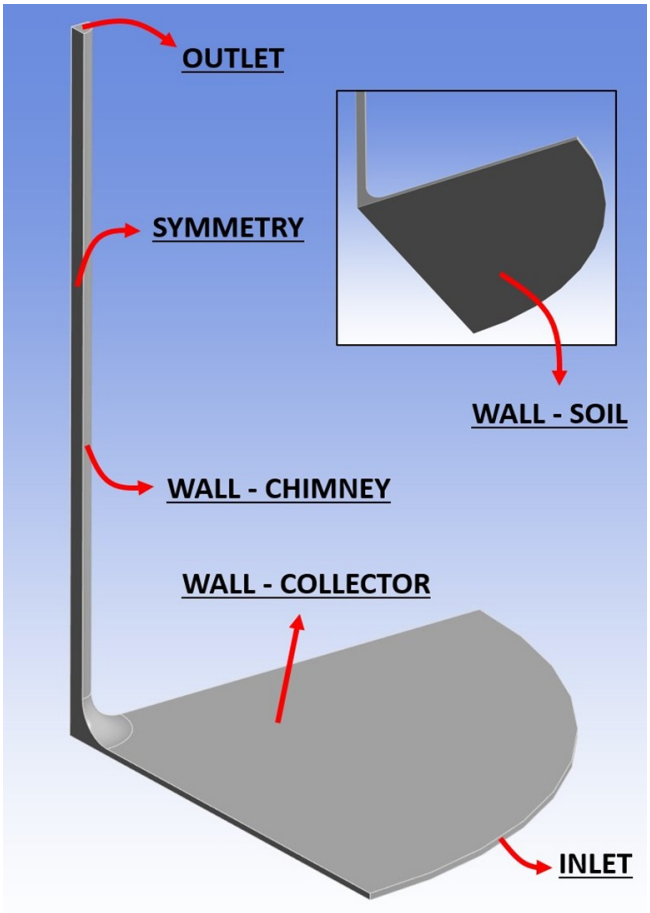

Figure 1. Simplified computational domain of a solar chimney power plant. Boundary conditions are indicated: inlet (air entry), outlet (ambient pressure outlet), collector and chimney walls, wall–ground interface, and the symmetry plane used in the computational fluid dynamics simulation.

a large collector-to-chimney area ratio is an essential control parameter for mass flow. These insights guided the selection of factors for the study. The following sections describe the methodology employed (Section 2), present and analyse the results obtained (Section 3), discuss their implications for optimization and control of SCPPs (Section 4), and finally offer conclusions and design recommendations drawn from the study (Section 5).

2. Materials and methods

The methodology consisted of two main stages: (i) validation of the CFD model against experimental data from the Manzanares pilot plant (using literature benchmarks), and (ii) a parametric analysis through statistical experimental designs aimed at optimizing the chimney's performance. In what follows, we detail the mathematical model and CFD simulation setup, the performance metrics and theoretical analysis, and the experimental design schemes used to systematically evaluate results.

2.1. Computation fluid dynamics model and simulation setup

Governing equations: The airflow and heat transfer in the solar chimney were modeled by the conservation equations of mass, momentum, and energy for a low-Mach, variable-density fluid under turbulent regime.[30] Axisymmetric flow in cylindrical coordinates (r, z) was assumed (neglecting any azimuthal variation, $v_\theta = 0$). Although the numerical solution was run to steady-state (time-invariant), the equations are presented in general form for clarity.

- Continuity (Mass Conservation): For variable density, in cylindrical coordinates the continuity equation is:

$$\frac{\partial \rho}{\partial t} + \frac{1}{r}\frac{\partial(\rho\, r\, v_r)}{\partial r} + \frac{\partial(\rho\, v_z)}{\partial z} = 0, \qquad (1)$$

  where ρ is air density and (v_r, v_z) are the radial and vertical velocity components.
- omentum Conservation: In the radial (r) and vertical (z) directions, the momentum equations are:

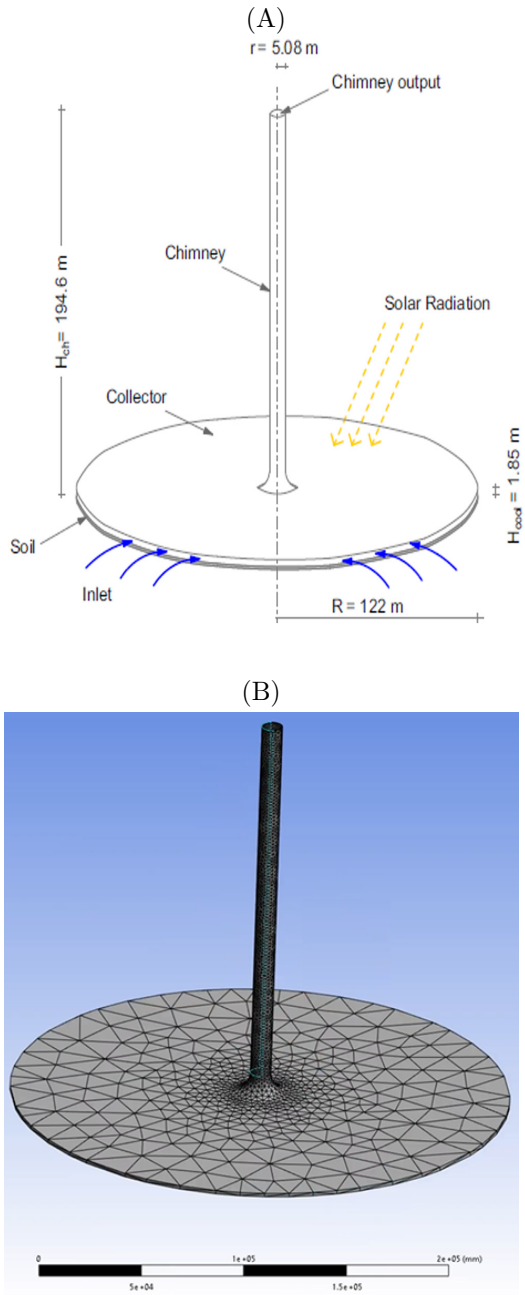

Figure 2. Details of the model and mesh used in the computational fluid dynamics analyses: (A) Geometric schematic and (B) generated mesh

$$-\frac{\partial p}{\partial r}+\mu\left[\frac{\partial}{\partial r}\left(\frac{1}{r}\frac{\partial(rv_r)}{\partial r}\right)+\frac{\partial^2 v_r}{\partial z^2}-\frac{v_r}{r^2}\right] = \rho\left(v_r\frac{\partial v_r}{\partial r}+v_z\frac{\partial v_r}{\partial z}\right), \quad (2)$$

$$\rho\, g-\frac{\partial p}{\partial z}+\mu\left[\frac{1}{r}\frac{\partial}{\partial r}\left(r\frac{\partial v_z}{\partial r}\right)+\frac{\partial^2 v_z}{\partial z^2}\right] = \rho\left(v_r\frac{\partial v_z}{\partial r}+v_z\frac{\partial v_z}{\partial z}\right), \quad (3)$$

where p is static pressure, μ the dynamic viscosity, and g the acceleration due to gravity.

- Energy Conservation: The energy equation includes conduction and radiative heat transfer:

$$\frac{\partial(\rho C_p T)}{\partial t}+\nabla\cdot(\rho C_p \mathbf{v}\, T)=\nabla\cdot(\lambda\nabla T)-\nabla\cdot\mathbf{q}_r, \quad (4)$$

where T is temperature, C_p the specific heat at constant pressure, λ the thermal conductivity, and $\mathbf{q}_r$ the radiative heat flux.

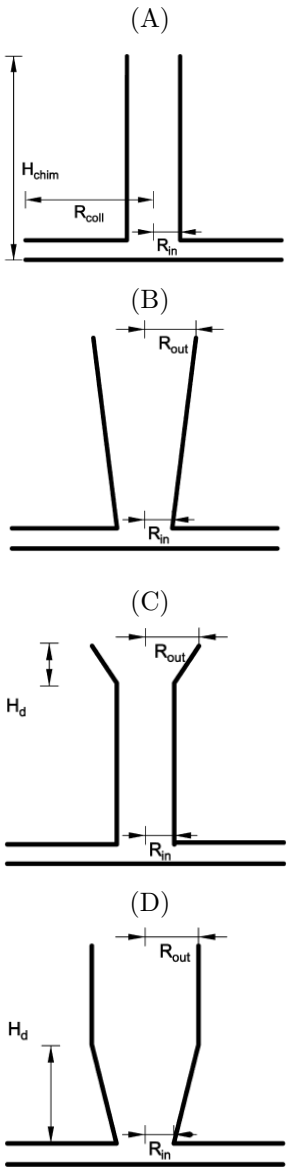

Figure 3. Typical geometric configurations of solar chimneys according to tower shape: (A) cylindrical, (B) divergent, (C) divergent with outlet expansion, and (D) divergent with base expansion

Turbulence and Radiation Models: Equations (1)–(4) were solved over the collector and chimney domain using ANSYS Fluent. Turbulence was modeled with the RNG k–ε scheme, which is suitable for buoyancy-driven convection flows, and radiative exchange was modeled using the discrete ordinates (DO) radiation model.[10] Air was treated as an ideal gas with temperature-dependent density; the Boussinesq approximation was applied for buoyancy terms to account for thermal density variation. A solar load model with an insolation of 1,000 W/m^2 (representative of clear noon conditions) was activated, and the solution was iterated to steady state.

Base Case Geometry and Mesh Independence: For validation, the Manzanares plant dimensions were replicated (see Table 1 for key geometry parameters, based on Haaf.[7,8]) The computational domain (comprising the circular collector and the chimney) was discretized primarily with tetrahedral elements, which effectively represent curved surfaces (Figure 2B). A local mesh refinement was applied near critical regions (collector inlet, ground, chimney walls) with element sizes ∼0.75 m, smoothly coarsening elsewhere. The final mesh contained $\sim 3.8\times10^5$ elements. Mesh independence was verified by comparing velocity and pressure profiles along the chimney height for progressively finer meshes (0.1M, 0.2M, 0.38M elements). The variations in peak velocity were under 1% beyond $\sim 3.8\times10^5$ elements, confirming that the adopted discretisation was sufficient (see Table 2 for mesh refinement results). All simulations were run until residuals stabilized and no further changes in monitored outputs were observed (Figure 4A–D).

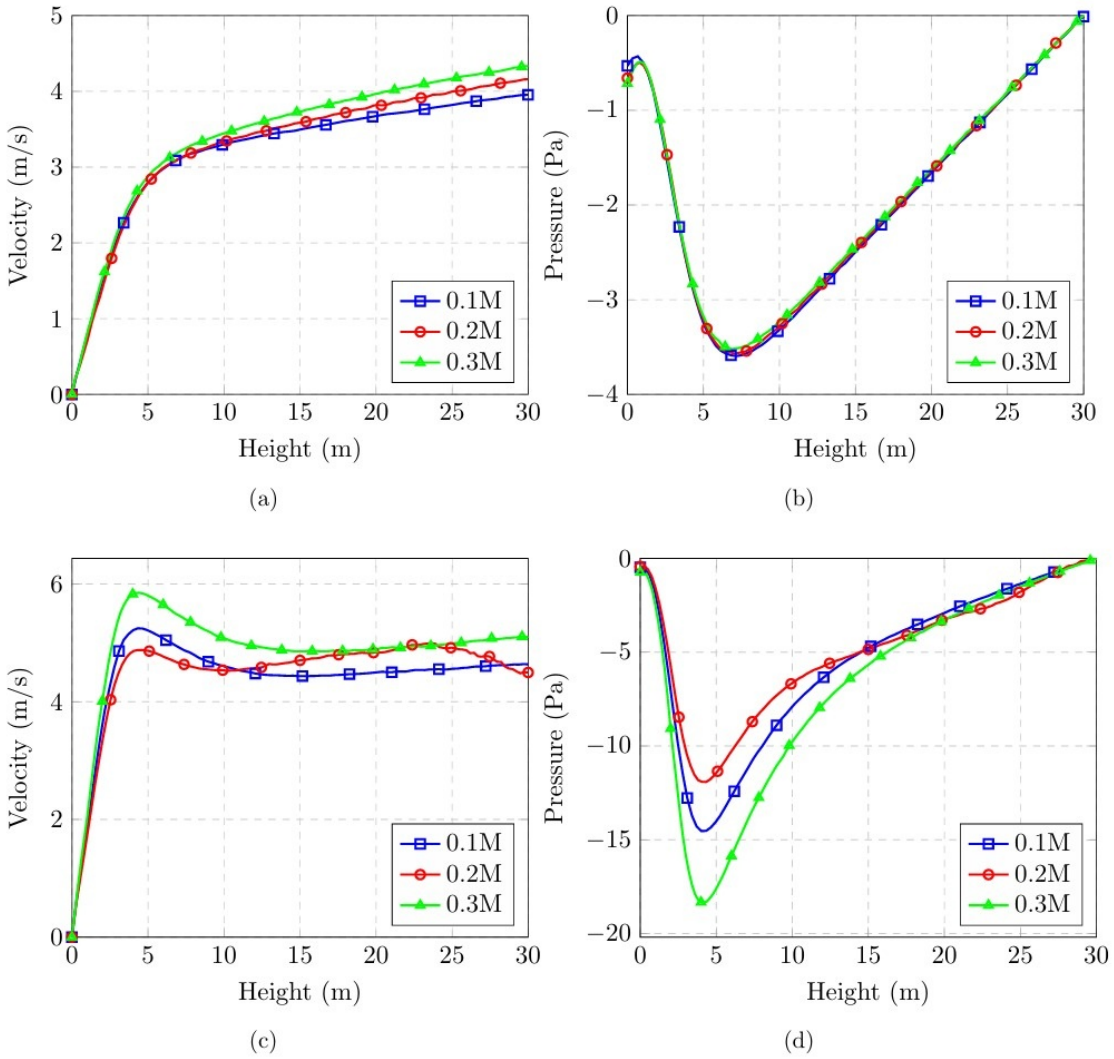

Figure 4. Mesh independence test in terms of velocity and pressure:
(A) velocity in convergent chimney, (B) pressure in convergent chimney, (C) velocity in divergent chimney, and (D) pressure in divergent chimney

Table 1. Main geometric parameters of the Manzanares (Spain) solar chimney pilot plant

Scale	H_{chim} (m)	R_{chim} (m)	H_{col} (m)	R_{col} (m)
Full (1)	194.6	5.08	1.85	122

Source: Haaf *et al.* [7,8]

Table 2. Results of the mesh independence test

Elements	Velocity (m/s)	Error (%)
3.76×10^5	14.6	2.66
3.79×10^5	14.8	1.33
3.83×10^5	14.9	0.66

Boundary Conditions and Verification: The inlet (collector edge) and outlet (chimney top) boundaries were set to ambient static pressure (0 Pa gauge) with $T_a = 302$ K.[8] The ground under the collector was modeled as an opaque heated wall (average surface temperature 327 K, emissivity $\alpha = 0.9$, absorptivity $\beta = 0.9$); the collector cover was defined as a semi-transparent wall (initial temperature 302 K, $\alpha = 0.9$, $\beta = 0.03$, transmissivity $\tau = 0.9$) following ref.[23] The chimney walls were assumed adiabatic. Tables 3 and 4 summarize all the boundary conditions applied without modification.

Table 3. Boundary conditions applied in the simulation.

Surface	Boundary condition
Inlet	Pressure–velocity
Outlet	Pressure–velocity
Ground	Mixed surface (opaque)
Collector	Mixed surface (semi-transparent)
Chimney	Adiabatic surface (opaque)

Table 4. Defined parameters for each surface.

Surface	Parameters
Inlet	$P = 0$ Pa, $T_a = 302\,\mathrm{K}$
Outlet	$P = 0$ Pa, $T = 300\,\mathrm{K}$
Ground	$T = 327\,\mathrm{K}$, $\alpha = 0.9$, $\beta = 0.9$
Collector	$T = 302\,\mathrm{K}$, $\alpha = 0.9$, $\beta = 0.03$, $\tau = 0.9$
Chimney	$\beta = 0$

Abbreviations: α = Emissivity; β = Absorptivity; τ = Transmissivity.

Model Validation: The CFD model was first validated against known performance data of the Manzanares chimney. Key outputs such as the maximum air velocity inside the chimney and the pressure drop between the collector inlet and chimney outlet were compared to experimental values reported by Haaf.[8] The CFD results reproduced the ∼15 m/s peak updraft velocity observed in Manzanares to within ∼5% error, and captured the qualitative pressure distribution along the tower. Additionally, trends reported by more recent CFD studies were replicated when varying mesh resolution, supporting the robustness of the numerical configuration.[23] This agreement with both historic and contemporary references builds confidence that the model can reliably predict solar chimney behaviour.

Convective regime: The characteristic Rayleigh number beneath the collector was estimated as

$$Ra = \frac{g\,\beta\,\Delta T\,H_{\mathrm{col}}^3}{\nu\,\alpha}, \tag{5}$$

where $\beta \approx 1/T$ is the thermal expansion coefficient, ΔT is the maximum air–wall temperature difference, H_{col} is the collector height, ν the kinematic viscosity, and α the thermal diffusivity. A value of $Ra \sim 10^9$ was obtained, which exceeds the typical threshold ($\sim 10^8$) for the onset of turbulence in free convection,[13] thereby justifying the use of a turbulence model.

2.2. Performance equations and power calculation

The performance of the solar chimney was quantified using classical expressions for power as a function of air mass flow rate and the pressure drop available at the turbine.[15] The mass flow rate $\dot{m}$ through the turbine is related to the volumetric flow rate V and the air density ρ by:

$$\dot{m} = \rho V \tag{6}$$

The theoretical extractable power, considering a turbine efficiency η_{turb} and a fraction χ of the thrust pressure effectively harnessed, is expressed as:

$$P = \eta_{\mathrm{turb}}\,\chi\,\sqrt{1-\chi}\,\Delta p_{\mathrm{pot}}\,V, \tag{7}$$

where Δp_{pot} denotes the total pressure difference generated by the chimney effect. This expression is derived from Bernoulli's principle, with χ optimized to maximize power, which typically occurs around $\chi \approx 2/3$.[15]

In practice, when χ is not optimized, power can be estimated using:

$$P \approx \eta_{\mathrm{turb}}\,\Delta p_{\mathrm{turb}}\,V, \tag{8}$$

where Δp_{turb} corresponds to the static pressure drop measured across the turbine.

In this study, power was calculated from CFD results using Equation (8), assuming a turbine efficiency of $\eta_{\mathrm{turb}} = 0.8$, as reported in Ref.[5] The flow rate V and pressure drop Δp_{turb} were extracted directly from each simulation for the various configurations analyzed.

2.3. Theoretical parametric analysis

As a methodological foundation for optimization, a simplified theoretical analysis was developed to understand how certain geometric ratios influence the solar chimney's flow behaviour. One key ratio is the area expansion factor between the chimney base and outlet, defined as:

$$\tau = \frac{A_t}{A_b}, \tag{9}$$

where A_b is the cross-sectional area at the chimney base and A_t at the top. For a cylindrical chimney $\tau = 1$, while a divergent chimney yields $\tau > 1$ due to the larger outlet diameter.

(1) Continuity and area ratio: Under steady conditions with essentially one-dimensional flow, mass continuity dictates that the volumetric flow rate is constant along the chimney:

$$A_b v_b = A_t v_t,$$

where v_b and v_t are the average air velocities at the base and top of the chimney, respectively. It follows that

$$\frac{v_b}{v_t} = \tau, \tag{10}$$

meaning that in a divergent chimney ($\tau > 1$), the air velocity near the base is higher than at the exit.

(2) Buoyancy-driven pressure potential: The driving force for the upward flow can be represented as an effective pressure differential between the base of the chimney and the ambient atmosphere at the top. This pressure potential is defined as:

$$\Delta P = P_0 - P_b, \tag{11}$$

where P_0 is the ambient atmospheric pressure at ground level, and P_b is the static pressure of the flow at the chimney base (both in Pa).[15,31]

(3) Energy balance (Bernoulli's principle): Assuming incompressible flow, Bernoulli's equation can be applied from a point b at the collector base to a point t at the chimney outlet (height H_{chim}):

$$P_b + \tfrac{1}{2}\rho v_b^2 = P_t + \tfrac{1}{2}\rho v_t^2 + \rho g H_{\text{chim}}, \qquad (12)$$

where P_t is the static pressure at the chimney top. At the outlet, P_t is approximately equal to P_0 (atmospheric pressure at that altitude, since the air leaving the chimney mixes with the ambient air and its velocity dissipates). The density of the internal air ρ is slightly lower than the ambient density ρ_0 due to solar heating. If we take $P_t \approx P_0 - \rho_0 g H_{\text{chim}}$ (accounting for the hydrostatic pressure drop in the outdoor air over the chimney height), Bernoulli's equation yields:

$$P_0 - P_b = (\rho_0 - \rho)\, g H_{\text{chim}} + \tfrac{1}{2}\rho\left(v_b^2 - v_t^2\right), \quad (13)$$

The left-hand side is exactly ΔP from Equation (11), so Equation (13) expresses the chimney's driving pressure ΔP as the sum of a buoyancy-induced term and a dynamic term (from the change in kinetic energy).

(4) Influence of Chimney Divergence (τ): Substituting the continuity relation (Equation 10) into Equation (13) gives:

$$\Delta P = (\rho_0 - \rho)\, g H_{\text{chim}} + \tfrac{1}{2}\rho v_b^2\left(1 - \tau^{-2}\right). \quad (14)$$

According to Equation (14), a greater area ratio ($\tau > 1$) increases the available pressure boost, since the second term is positive for $\tau > 1$. In other words, a divergent chimney can generate a larger pressure-driven suction than a cylindrical one ($\tau = 1$, for which the dynamic term vanishes and ΔP depends solely on buoyancy). The dynamic contribution $\frac{1}{2}\rho v_b^2(1-\tau^{-2})$ becomes significant only if the base velocity v_b exceeds a threshold on the order of 1 m/s; below that, the effect is marginal. In our case study, expected solar-induced updrafts (and any local winds) ensure $v_b > 1$ m/s, meaning a divergent chimney's theoretical advantage can be realized. Indeed, climatological data for the Lambayeque region report typical wind speeds of ∼2.5 m/s (with daytime minima around 1.5 m/s.[32]), confirming that this condition is likely met.

Relevance to optimization and control: This theoretical analysis establishes three fundamental principles for design optimization: (i) a divergent chimney geometry (large τ) increases the available thrust (pressure differential), (ii) a taller chimney height H_{chim} amplifies the buoyant draft effect, and (iii) the collector-to-chimney area ratio (or equivalently AR) is a critical control parameter for the system's mass flow and power. These guidelines clarify the underlying physics and provide quantitative criteria to guide design strategies. In essence, they indicate that maximizing the collector area and employing an expanding chimney should yield higher performance, while chimney height also plays a major role-all of which will be explored in detail via CFD experiments.

2.4. Experimental design and parameters

To exhaustively explore the design space of the solar chimney and ensure reliable outcomes, we applied multiple types of statistical experimental design.[33] In total, 11 different design structures were implemented, including: a randomized complete block design (RCBD), a two-factor analysis of variance (ANOVA) (with mixed factors), a three-factor ANOVA (with fixed factors), a Latin square design, a two-level fractional factorial design, a Graeco-latin Square design, a balanced incomplete block design (BIBD), a general linear model (GLM) regression, a nested design, a split-plot design, and a factorial analysis on an unbalanced dataset. These diverse methodological approaches covered a wide range of scenarios, exploring both interactions between factors and the effects of blocking variables. Comparing findings across multiple analysis methods ensures that the identified optimal configuration is not an artefact of any single approach, thereby demonstrating the versatility and consistency of our strategy.

The factors considered across these designs included both geometric features and environmental/material parameters of the solar chimney system:

- Collector-to-chimney area ratio (AR): Defined as the ratio of the collector area to the chimney cross-sectional area. High area ratio (AR) corresponds to a much larger collector relative to the chimney, which in theory enhances the volume of heated air available for driving the turbine.
- Chimney geometry: Different chimney shapes were tested: Cylindrical (CC) with constant diameter, divergent (DC) with expanding diameter toward the top, and in some designs also a conical (Co) variant (a straight truncated cone) to contrast with the curved hyperbolic divergence of the DC shape.
- Chimney height: In certain designs (e.g. Latin and Graeco-Latin squares), multiple chimney heights (e.g., 20 m, 30 m, 40

m) were evaluated to quantify the effect of height on performance.

- Collector size (implicit in AR): By varying AR, the collector radius/area was effectively changed relative to a given chimney diameter. In our simulations, a high AR (such as 6) indicates a very large collector (e.g., ∼90 m radius) compared to the chimney diameter (∼10 m), whereas lower AR (2 or 4) use smaller collectors.
- Turbine presence: Some experiments (e.g., the three-factor ANOVA) included a factor for turbine presence vs. absence to assess how having an energy-extracting turbine (with an assumed efficiency) affects the airflow and power.
- Chimney material: One of the designs (the Graeco-latin square) incorporated material thermal properties by testing different chimney wall materials (e.g., a high thermal inertia material like concrete vs. a lighter metal), to evaluate whether material thermal capacity influences performance.
- Environmental conditions (Region/climate): A two-factor ANOVA was dedicated to regional climatic differences, using three different sets of ambient conditions (denoted Region 1, 2, and 3) representing variations in solar irradiance, air temperature, and wind typical of coastal vs. inland conditions in Lambayeque. Additionally, the split-plot design introduced time-of-day (morning/afternoon) and season (winter/summer) blocks, to simulate how diurnal and seasonal changes might impact performance.

Each of the 11 experimental designs organized these factors in different ways (for example, by assigning certain factors to blocks or main plots, or by using fractional subsets of combinations). In total, 66 CFD simulation cases were executed, corresponding to different combinations of factor levels as prescribed by the designs. The power output P of the solar chimney (mechanical power available to the turbine, in kW) was recorded for each simulation as the primary response variable. Statistical analysis was then performed using R software: Analyses of variance (ANOVAs) to determine the significance of main effects and interactions, Tukey post-hoc tests for pairwise comparisons where appropriate, and fitted linear models to estimate the relative influence of each factor. Specialized procedures were employed for the more complex designs (Latin square, Graeco-Latin, nested, split-plot) to ensure correct interpretation of effects according to their structure. By comparing results across the multiple designs, we could verify that the optimal configuration identified is consistent and statistically robust, rather than an artefact of any single experimental setup. Moreover, each design provided additional insights; for example, the Graeco-Latin square isolated the influence of chimney material, while the incomplete block design demonstrated that optimization outcomes can be drawn even when not all factor combinations are tested.

In summary, employing such a broad array of experimental designs was aimed at obtaining reliable and generalizable outcomes. The convergence of evidence from these methods increases confidence that the performance trends observed (and the optimal design parameters identified) are genuinely due to the physics of the system and not dependent on any one analytical approach. The following section presents the results from these simulations, organized by each experimental design, and highlights the key findings.

The geometric configurations analyzed via CFD were defined based on the base geometry of the Manzanares plant (Table 1), scaled according to the required collector area and chimney height levels. For practical reasons, the collector radius was adjusted to achieve the desired area ratio (for example, for AR = 6, the collector radius was increased while maintaining the base chimney radius constant). In all parametric simulation cases, typical ambient conditions for Lambayeque were considered: ambient temperature $T_a = 296.65$ K (23.5°C), atmospheric pressure $P_{\text{amb}} \approx 93.9$ kPa, solar irradiance of 850 W/m^2, and an absorbed ground heat flux beneath the collector of approximately 250 W/m^2. These values correspond to daily full-sun averages in the region, obtained from climatological databases (NASA-POWER[32] and RETScreen.[24]) The same physical model configurations (turbulence and radiation models) as in the base simulation were applied, with the mesh adapted to each new geometry.

In addition to the classical CFD and statistical DOE techniques applied in this study, it is worth acknowledging the growing use of advanced analytical frameworks in contemporary optimization research. Recent works have explored fuzzy set–based multi-criteria decision metrics and fractional-order differential models to characterise the behaviour and stability of complex dynamical systems.[34–36] Although these methods originate from distinct application domains, they illustrate modelling strategies that

could complement future analyses of solar chimney performance—particularly for transient thermal–flow dynamics or intelligent control optimization. While the present study does not implement these approaches, recognizing them situates our methodology within the broader landscape of modern modeling and optimization tools.

2.5. Post-processing and results analysis

For each experimental design, the power response P was analyzed as a function of the factors. ANOVAs were conducted to determine the statistical significance of the main effects and their interactions. Where relevant, post-hoc tests were applied to compare means across levels (e.g., to determine which AR level produced significant differences in power). Designs with special structures (Latin square, Graeco-Latin, nested, split-plot) were analyzed using the appropriate statistical procedures for each case, ensuring correct interpretations. Additionally, a general linear model (GLM) was fitted using all the data to quantify the contribution of each factor in terms of estimated coefficients.

The combined use of classical and advanced design techniques ensured both statistical validity and the ability to generalize findings to different operating scenarios. The results from all these evaluations were cross-compared to identify consistent trends. In particular, attention was given to determining which combination of geometric parameters produces the maximum power in the solar chimney, and whether this combination remains consistent regardless of the analysis method used. The global findings are summarized in the following section.

3. Results

The 11 experimental designs defined in the methodology resulted in a total of 66 CFD simulation runs. This section reports the outcomes of those simulations, organized by each specific design, followed by a comparative analysis and context with prior literature. Despite examining different subsets of factors, all 11 design analyses led to broadly congruent conclusions, reinforcing the robustness of the observed trends. Table A1 Appendix summarizes, for each design, the combination of parameters that yielded the highest power and the value of that power, along with the key factors identified and any notable observations. Below, we briefly describe the main findings of each experimental design:

(1) Randomized complete block design (RCBD): This design evaluated combinations of AR levels (AR = 2, 4, 6) and chimney type (CC vs. DC), with replicates blocked by run order. The base geometry was a DC of height $H = 40$ m, base diameter $D_b = 5.00$ m and top diameter $D_t = 12.40$ m, with a collector radius $R_{col} = 90$ m and cover height 1.85 m. The maximum power recorded was ∼16 kW, obtained with AR = 6 and a DC. This confirmed that enlarging the collector area (a 6:1 AR relative to the chimney) substantially improves the heated airflow, while the DC shape provides an additional boost to energy extraction (see Figure 5). By contrast, configurations with lower AR experienced a marked drop in power (down to ∼7–10 kW), underscoring the strong influence of collector area on overall performance.

(2) Two-factor ANOVA (AR × region): This design considered two levels of AR (AR = 2 and 6) across three different regional climate scenarios (Region 1, 2, and 3), to identify the influence of environmental context on system performance. The geometry used was a DC of $H = 20$ m ($D_b = 5.00$ m, $D_t = 12.40$ m) with a collector $R_{col} = 90$ m (cover height 1.85 m). Results showed that AR = 6 outperformed AR = 2 in all climates, with the highest power ∼12 kW achieved under Region 2 conditions. Region 2 (representing warmer, high-irradiance conditions) produced better performance, suggesting that higher solar input and ambient temperature enhance the chimney's output. No significant interaction was found between AR and region, indicating that the beneficial effect of a larger collector is consistent across different climatic backgrounds (see Figure 6).

(3) Three-Factor ANOVA (AR × Chimney Type × Turbine): Here, two ARs (2, 6), two chimney geometries (CC, DC), and turbine presence/absence were varied to quantify their combined effect on power. The base model geometry was a DC of $H = 30$ m ($D_b = 5.00$ m, $D_t = 12.40$ m) with a collector $R_{col} = 90$ m (cover 1.85 m). CFD results showed that AR = 6 with a DC yielded the highest power, reaching about 15 kW when no turbine was present. Including the turbine (modeled as an energy extraction inducing pressure drop) reduced the power by ∼10–15%, down to ∼13 kW, due to mechanical energy being drawn off-but importantly without changing the ranking of the other factors. In fact, each factor individually (AR, chimney type, turbine) had a

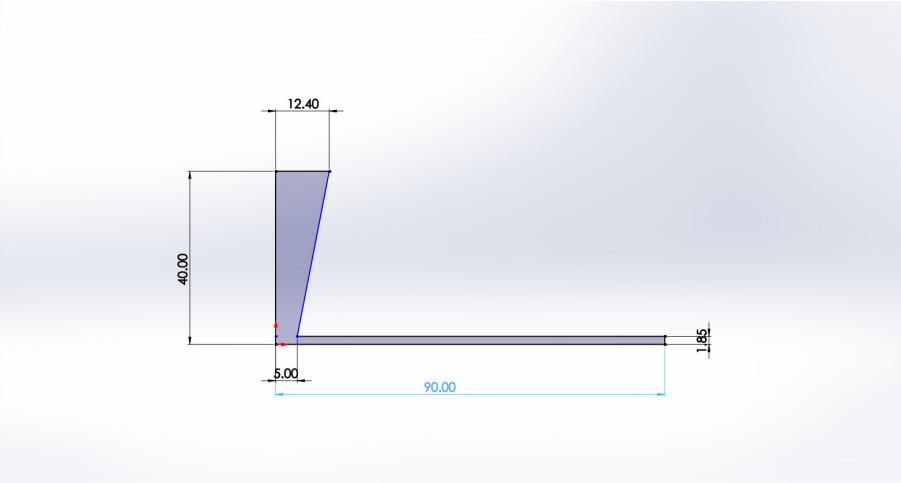

Figure 5. Power output for area ratios (AR = 2, 4, 6) and chimney types in the randomized complete block design. The AR = 6 divergent configuration delivers the highest output (∼16 kW), while smaller ARs produce substantially less power

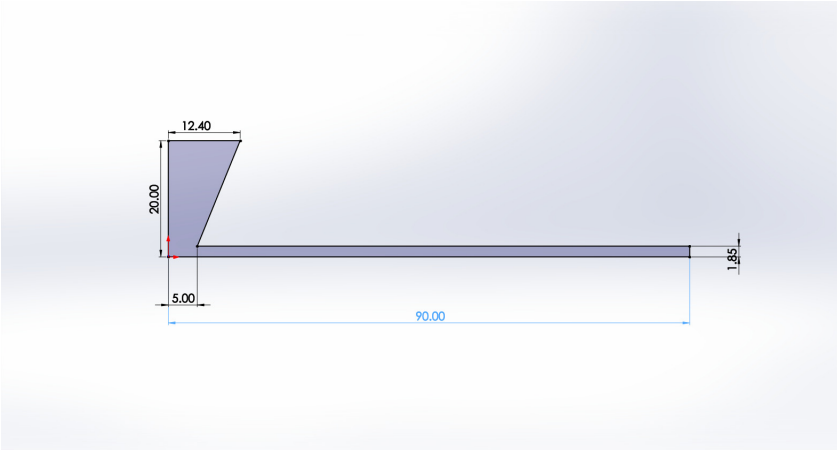

Figure 6. Effect of AR (2 vs. 6) on power output under three different regional climate conditions (two-factor ANOVA results). In all climates, the higher AR (AR = 6) outperforms AR = 2, confirming the consistency of the AR benefit across varied environments.
Abbreviation: AR: Area ratio.

statistically significant main effect, and no strong interactions between them were detected. The turbine's penalty was similar for both chimney shapes and AR levels, confirming that the aero-thermal behaviour of the system remains stable despite the turbine load. Overall, this design reinforced that a high AR and DC maximize power, and that the presence of a turbine, while reducing absolute power, does not negate the advantages of the optimal geometric design (see Figure 7).

(4) Latin square design (LSD): A 3 × 3 Latin square was applied to orthogonally evaluate the main effects of AR (AR = 2, 4, 6), chimney height (e.g., 20, 30, 40 m), and chimney geometry (CC, DC) while reducing the total number of simulations required. The representative geometry for this set was a smooth DC of $H = 30$ m ($D_b = 4.00$ m, $D_t = 9.80$ m) with a collector $R_{col} = 90$ m (cover height 1.85 m). Results showed that the configuration with AR = 6 and a DC again produced the highest power, approximately 14–15 kW. In contrast, combinations with lower AR (2 or 4) yielded much lower power in the ∼8–10 kW range. This statistically controlled design verified that AR and chimney type are the most influential factors affecting performance, consistent with the patterns observed in the full factorial experiments (see Figure 8).

(5) Graeco-latin square design: This 3 × 3 design enabled the simultaneous study of four factors (each at three levels) by treating two factors as Latin and two as Greek variables. The factors were AR (2, 4, 6), chimney height (20, 25, 30 m), chimney type (CC, DC, Co), and

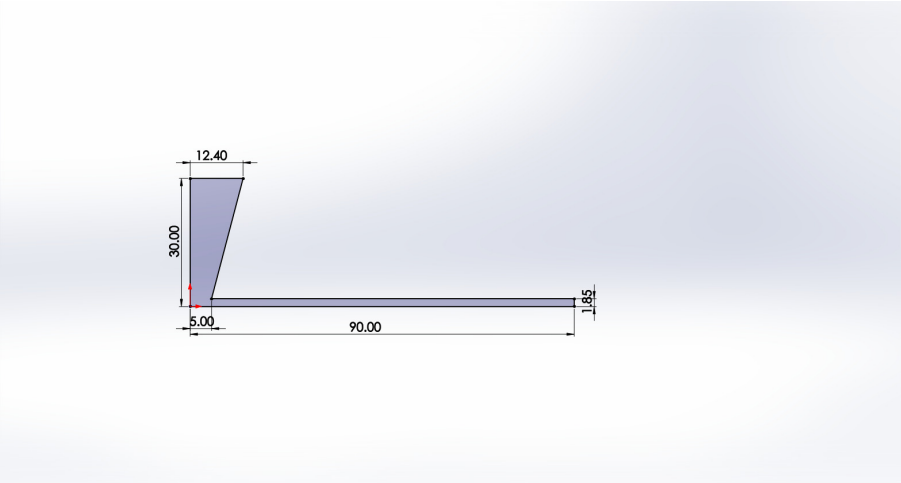

Figure 7. Main effects of area ratio (AR), chimney type, and turbine presence on power output (three-factor ANOVA results). The plot highlights that AR = 6 and a divergent chimney maximize power, while the inclusion of a turbine causes a modest reduction (by ∼10–15%) in output.

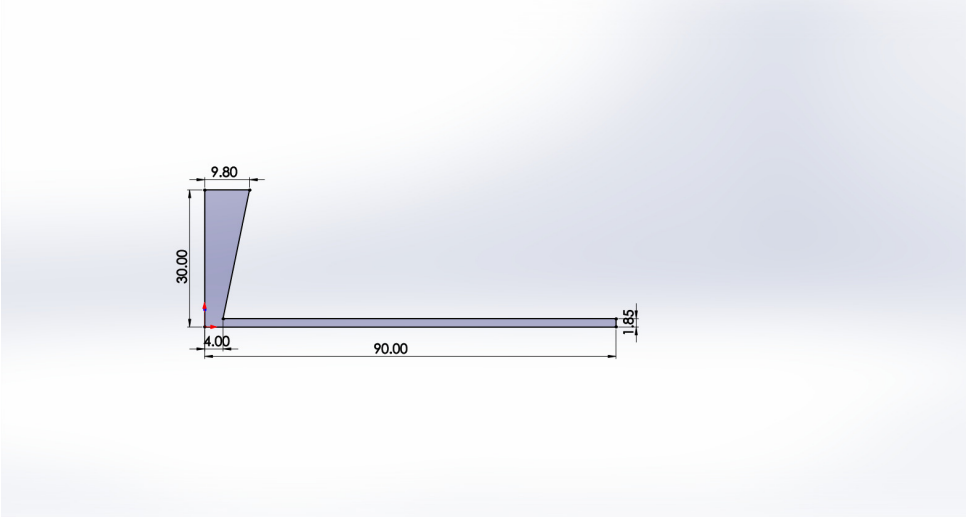

Figure 8. Latin square results showing the effects of area ratio, chimney height, and chimney shape on power output. The AR = 6 tall divergent chimney yields the highest output (∼14–15 kW), whereas lower AR or shorter chimneys produce only 8–10 kW.

material (aluminium, steel, concrete). The highest power occurred for AR = 6, height = 30 m, and a DC with the high-inertia material (concrete). The representative optimal run used a 30 m DC chimney (D_b = 6.00 m, D_t = 14.70 m) and R_{col} = 90 m, yielding about 15–16 kW. Variants with lighter materials or smaller AR produced lower power (∼11–13 kW), confirming that collector area and chimney divergence dominate the response, while material has a secondary but positive effect (Figure 9).

(6) Two-level fractional factorial (FrF_2): A fractional factorial 2^{3-1} design was run, considering AR (2, 6), chimney type (CC, DC), and a third geometric factor (N) representing the presence of an internal constriction or "neck" inside the chimney. The geometry studied had H = 30 m (D_b = 4.00 m, D_t = 9.80 m, collector R_{col} = 90 m), and a neck (constriction) was introduced at 20 m height in the chimney for the level "yes" of factor N. Despite using only half of the full factorial combinations, the principal effects were correctly identified: high AR and a divergent chimney increased power, whereas adding the internal neck (factor N) showed no statistically significant effect on output. The maximum power recorded in this subset was on the order of 13–14 kW, consistent with values from the equivalent full designs (see Figure 10).

(7) Balanced incomplete block design (BIBD): This design analyzed partial combinations of AR (2, 4, 6) and chimney type (CC, DC, Co) organized in incomplete blocks, such that not all pairs of levels were tested. The reference

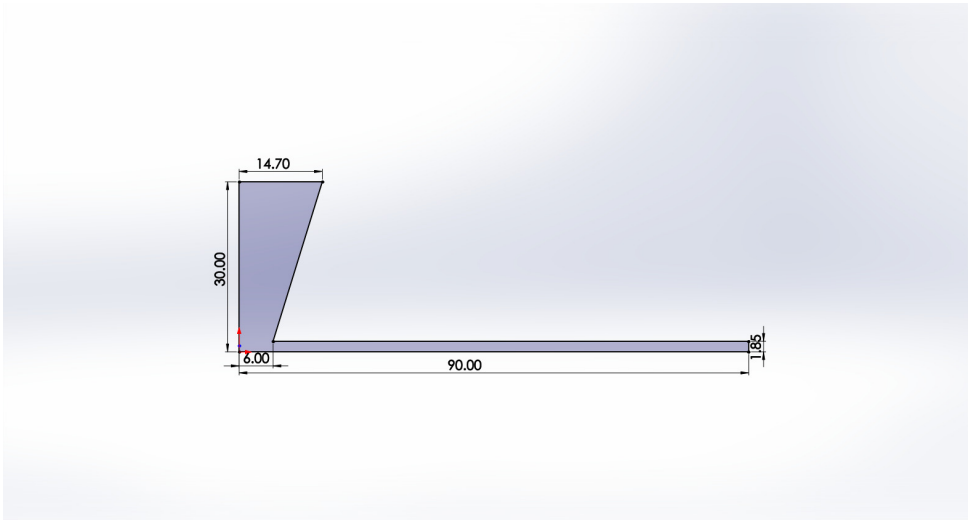

Figure 9. Graeco-Latin square results showing the combined effects of area ratio, chimney height, chimney shape, and material on power. The optimal case (AR = 6, 30 m divergent chimney, concrete walls) produced ∼15–16 kW, whereas lighter materials or smaller ARs yielded ∼11–13 kW.

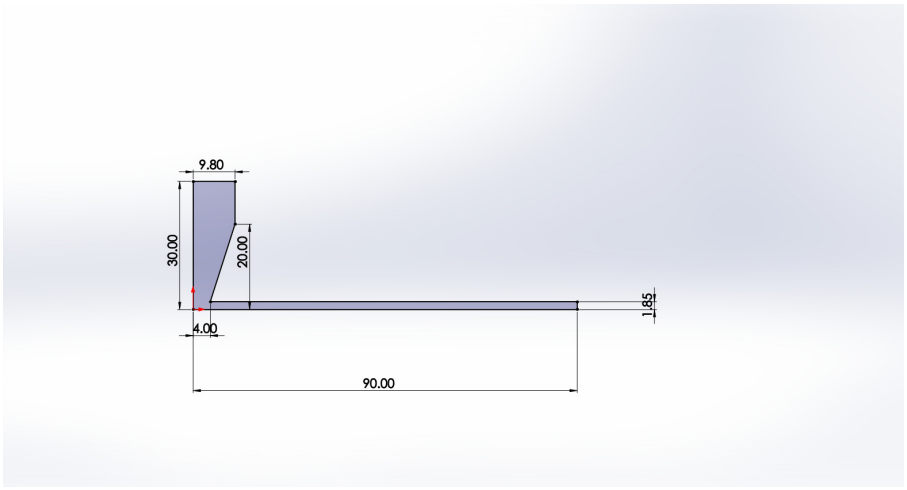

Figure 10. Two-level fractional factorial results for area ratio, chimney type, and neck presence show that high area ratio and a divergent chimney yield the greatest output (∼13–14 kW), while adding a neck has no significant effect.

geometry was a DC of $H = 30$ m ($D_b = 4.00$ m, $D_t = 9.80$ m, $R_{col} = 90$ m). Even with fewer runs than a full factorial, it was observed that the DC gave the highest power (∼15 kW), followed by the Co (∼11–12 kW). Configurations with AR = 2 or 4 did not reach those levels (only ∼9–10 kW). This incomplete analysis once again confirmed the superiority of a large collector and divergent tower, even under a reduced sampling scheme (see Figure 11).

(8) General linear model (GLM)-regression: A global regression model was fitted to the combined experimental dataset, quantifying the relative influence of each geometric factor on power. The representative geometry used for predictions was a DC with delayed expansion ($H = 30$ m, $D_b = 4.00$ m, $D_t = 9.80$ m, $R_{col} = 90$ m). The analysis showed that the AR is the dominant factor, followed by chimney divergence, while other parameters had only minor effects. The GLM predicted a maximum power of ∼13–14 kW, consistent with the general trend that larger AR and greater divergence increase mass flow and power. The model also interpolated unsimulated configurations, supporting the broader conclusions from the factorial designs (see Figure 12).

(9) Nested design: In this experiment, a nested structure was used to analyse variability among chimney geometries within each level of AR. The base geometry was a DC of $H = 30$ m ($D_b = 5.50$ m, $D_t = 13.50$ m, $R_{col} = 90$ m, cover 1.85 m). Each AR level (2, 4, 6) contained two variants of chimney

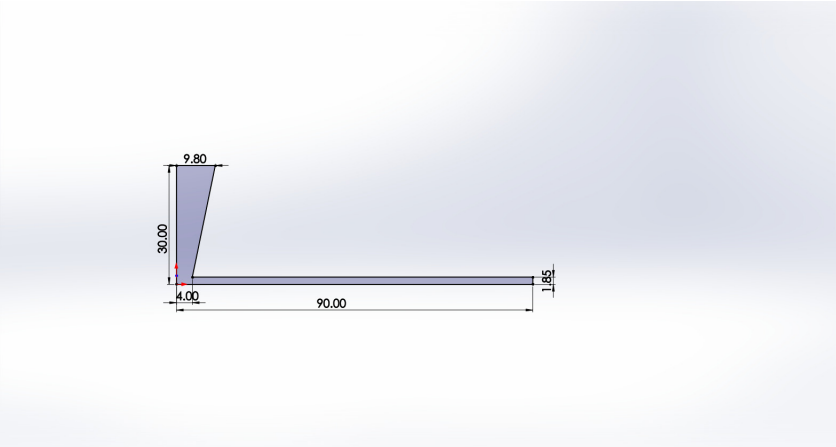

Figure 11. Balanced incomplete block design results showing that AR = 6, particularly with a divergent chimney, yields the highest power (∼15 kW), while lower AR configurations remain below ∼10 kW Abbreviation: AR: Area ratio.

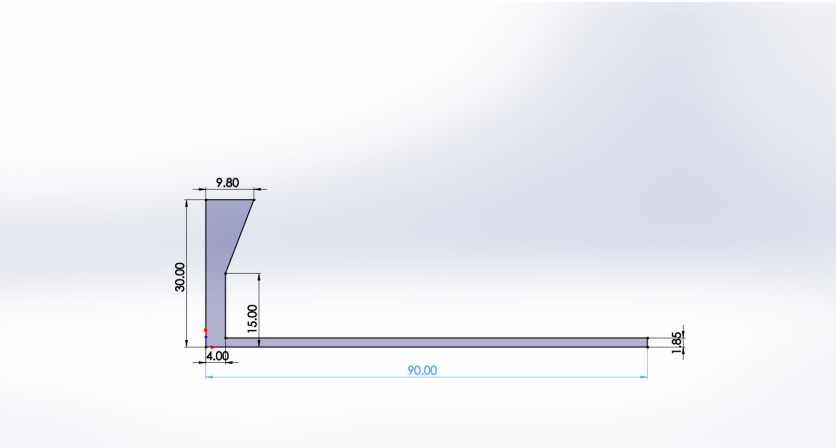

Figure 12. General linear model regression predictions of power output based on the aggregated experiments. The regression surface shows that a larger collector area ratio and a DC geometry exert the strongest positive influence on power.

shape (CC and DC) nested under that AR. The results showed that the highest power was attained for AR = 6 with a DC, with values around 15–16 kW. The nested design helped isolate the effect of geometry within each AR: it revealed moderate internal differences (DC outperforming CC within each AR level), consistent with the global patterns. This approach validated the stability of previous results and showed that even at a fixed AR, geometric modifications influence efficiency appreciably (see Figure 13).

(10) Split-plot design: A split-plot design was employed to study the effect of AR and chimney type under varying environmental blocks. Specifically, time-of-day (morning vs. afternoon) and season (winter vs. summer) were treated as block factors, simulating constrained field experiment conditions. The main-plot factor was the combined daily/seasonal condition, and the sub-plot factors were AR (2, 6) and chimney type (CC, DC). The principal geometry was a DC of $H = 35$ m ($D_b = 5.00$ m, $D_t = 12.30$ m) with $R_{col} = 90$ m. The CFD outcomes showed patterns consistent with previous designs: high AR and DC yielded the best performance, with a maximum of about 17–18 kW under the most favourable condition (e.g., summer midday). In contrast, the combination of AR = 2 and a CC produced only 8–9 kW. This design, meant to mimic real-world operational variations, confirmed that the conclusions drawn under controlled "laboratory" conditions are robust against environmental fluctuations-although the absolute power levels vary with solar irradiance and ambient temperature, the ranking of design choices remains the same (see Figure 14).

(11) Unbalanced factorial analysis: Finally, an aggregate analysis was performed on a combined dataset from different experiments that

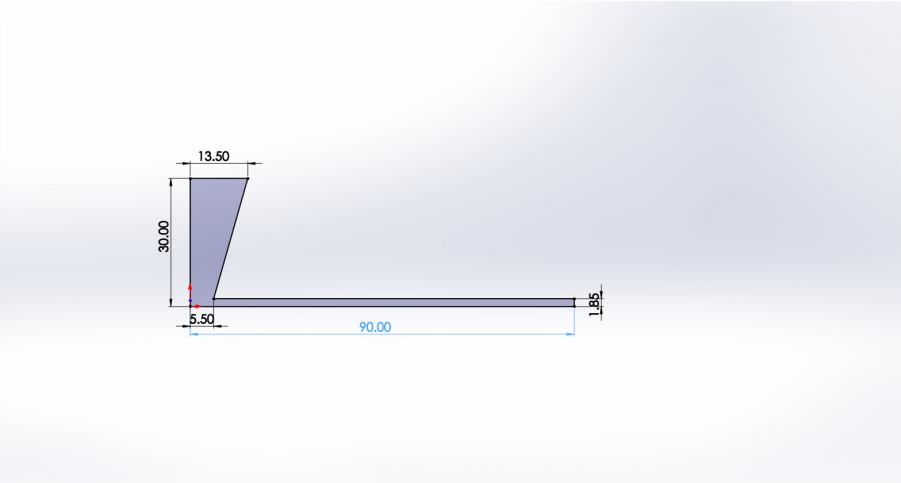

Figure 13. Nested design results: comparison of chimney geometry effects (cylindrical vs. divergent) within each area ratio level. For each fixed AR, a DC produces more power than a cylindrical one (e.g., ∼15–16 kW vs. ∼14 kW at AR = 6), although the magnitude of this geometry effect is smaller at low AR
Abbreviation: AR: Area ratio.

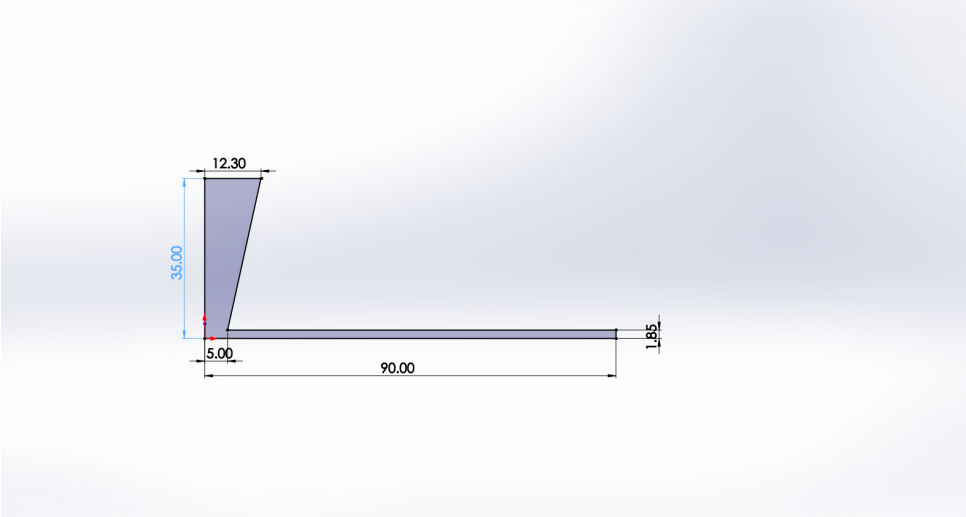

Figure 14. Split-plot design results showing power output across time-of-day and seasonal blocks for area ratios 2 and 6 and two chimney types. The high-area ratio divergent configuration consistently gives the highest output under all conditions, confirming its robustness against environmental variability

together covered various combinations of AR (2, 4, 6) and chimney types (CC, DC, Co), albeit in an unbalanced way (some combinations missing). Using a Generalized least squares (GLS) approach to handle the imbalance, it was found once again that AR = 6 with a DC delivers the highest power. In particular, for the representative geometry of this analysis (H = 25 m, D_b = 5.00 m, D_t = 12.30 m, $R_{col} \approx 90$ m), the peak power was ∼14 kW. The second-best combination was AR = 6 with a Co, at ∼11–12 kW, while any configuration with AR = 2 or 4 did not exceed ∼7–10 kW. This reinforces that even when pooling data from disparate sources (mimicking the situation of integrating results from multiple studies or prototypes), the trends are clear: increasing AR and using a divergent tower are the primary determinants of performance (see Figure 15).

3.1. Comparative analysis and statistical significance

Across all designs, the statistical analyses (ANOVA, etc.) consistently supported the direct simulation observations: AR and chimney type emerged as the most significant factors (with $p < 0.01$) determining the generated power. No strong interactions between the main factors were found in any design, suggesting that their effects are approximately additive over the range studied. Environmental conditions (different regions or blocks) did introduce variations in the absolute

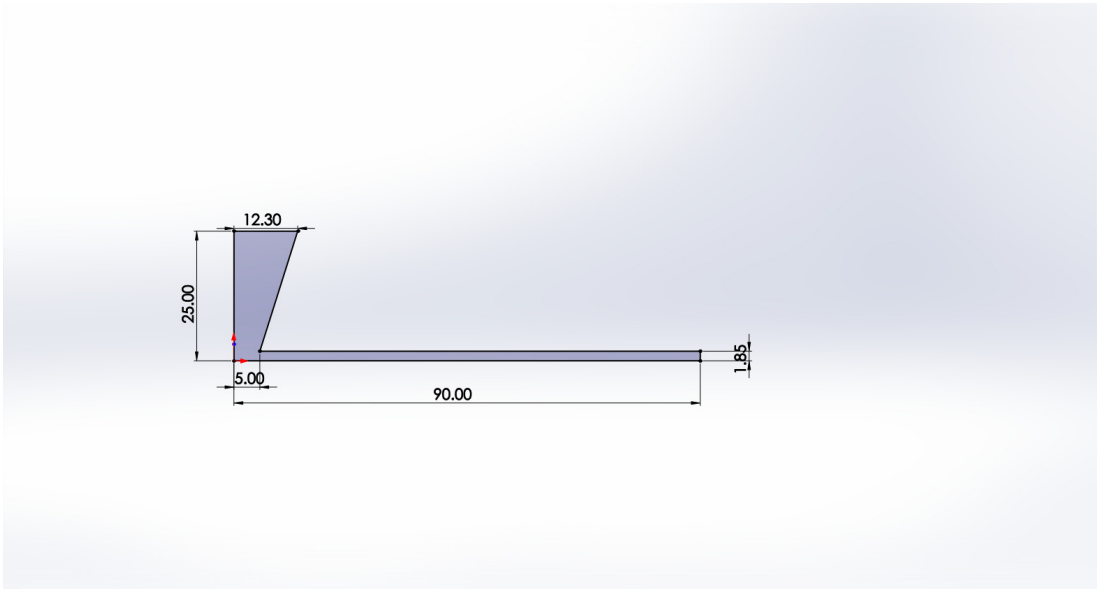

Figure 15. Unbalanced factorial analysis results showing that the AR = 6 divergent configuration delivers the highest power (∼14 kW), whereas smaller-AR cases (2 or 4) remain below ∼10 kW, reinforcing the dominant influence of collector area and chimney divergence
Abbreviation: AR: Area ratio

power levels-a warmer, sunnier scenario yielded higher power outputs overall-but crucially, they did not alter the efficiency hierarchy of the designs. In other words, an optimized configuration (high AR, DC) remained optimal regardless of ambient differences, though the magnitude of its power advantage scaled with the available solar resource.

We also compared our results with existing experimental data. For example, Haaf[8] reported that the Manzanares pilot plant (195 m tall, collector diameter ∼244 m) generated on the order of 50 kW. In our case, with only a 30 m tall chimney but a relatively oversized collector (AR = 6 implies a collector diameter of ∼60 m for a ∼10 m chimney diameter), we obtained power outputs in the tens of kilowatts-notably, ∼15 kW at optimum. This is on the same order of magnitude, despite the much smaller scale. Naturally, there are practical limits: an excessively large AR would eventually face diminishing returns due to thermal losses, and indefinitely increasing chimney height is infeasible for cost and structural reasons. Nonetheless, our results suggest that with optimized design, it is possible to maximize efficiency even at reduced scales, getting surprisingly good performance within realistic constraints. Additionally, a recent experimental prototype in Sfax, Tunisia demonstrated that solar chimneys can perform effectively even in arid climates, further supporting the viability of the concept in diverse environmental conditions.[37]

4. Discussion

4.1. Optimal design combination

Out of all the evaluated scenarios, the collector–chimney configuration with AR = 6 and a DC proved to be the most effective configuration. This combination made the most of the available solar energy, achieving power outputs on the order of ∼15 kW even in relatively modest-sized setups. By contrast, configurations with smaller collectors (low AR) and conventional CCs delivered far less power. For example, in the split-plot design the setup with a reduced collector and a CC produced only about 7 kW-roughly half of what the optimal design yielded under the same conditions. This quantifies the critical importance of a broad collector and an appropriate chimney geometry to enhance airflow and thereby energy extraction.

An interesting finding is that while the DC shape consistently benefited performance, its advantage was somewhat less pronounced than that of increasing the collector area. In designs where a convergent (inward-tapering) chimney was tested (labelled Co, a truncated cone narrowing toward the top), its performance fell in between the cylindrical and divergent cases (for instance, about 11 kW vs. 15 kW for the high-AR scenario). This indicates that a Co penalizes the flow (likely by incurring greater frictional losses and flow separation), reducing the extracted power compared to a divergent shape. On the other hand, the performance gap between cylindrical and DCs was modest when the collector was very small-in such cases, the system was so deprived airflow that

chimney shape made less difference. This suggests that the impact of chimney geometry becomes more relevant when a strong airflow is driven by a large collector; if the collector is undersized, improving the chimney design cannot compensate much for the lack of heated air.

4.2. Influence of secondary factors

The exploratory designs with special configurations (Latin squares, Graeco-Latin, etc.) included additional geometric tweaks-such as internal baffles, stepped sections, or other chimney modifications. None of these alterations yielded any significant increase in power; they mostly provided information on the limits of improvement. In essence, internal chimney modifications appear to have second-order effects compared to the primary parameters (AR and overall chimney shape). Similarly, the inclusion of a turbine (necessary for actual power generation) caused a slight drop in measured air power (on the order of 1 kW, roughly 10–15% relative). This drop corresponds to the mechanical energy that an ideal turbine would extract and convert to electricity, and is thus expected. Crucially, adding the turbine did not nullify the benefits of good aero-thermal design-even with a turbine in place, the configurations with higher AR and DCs continued to produce more power than the others. The turbine simply imposes a slightly lower ceiling on the usable power.

Regarding environmental conditions, comparing different ambient scenarios revealed that variations in air temperature and solar irradiation have an almost linear influence on generated power. For instance, the warmer Region 2 climate yielded up to ∼12 kW in the best design, versus slightly lower values in cooler regions. This outcome was anticipated (better solar resource yields more power). However, even under less favourable conditions, the order of performance remained the same-the high-AR divergent design was always superior. In other words, optimizing AR and chimney geometry is beneficial independent of the operating environment, even though the absolute gain will be larger in sunnier, hotter climates.

4.3. Limitations and validity of results

While our CFD simulations provide detailed performance estimates, they are based on idealized conditions. In practice, unmodeled factors could reduce the achievable power. For example, we assumed a clean collector cover with no dust accumulation; in reality, dust or dirt on the collector would gradually reduce its solar transmissivity and thus degrade performance. We also neglected external heat losses (e.g., convective losses from the collector edges to ambient air), which would diminish the thermal energy available to drive the updraft. Additionally, our analysis was steady-state at peak solar irradiance, without diurnal variation, whereas in real operation the power output would rise and fall over the day (peaking at solar noon and dropping in the morning and late afternoon). Furthermore, ambient wind conditions can influence the chimney's performance– a mild breeze entering under the collector can enhance airflow, whereas strong or turbulent winds might disrupt the thermal plume and reduce efficiency. Our simulations assumed still air, so field performance may differ depending on local wind patterns. It is important to emphasize that the maximum power values obtained in our models (on the order of 15 kW) assume a clean collector, high insolation, and near-optimal conditions; real-world net outputs would likely be lower due to dust, imperfect transmission, and other losses. Even so, the qualitative trends identified-such as the benefits of a large AR and a DC-are robust and aligned with physical intuition and the limited experimental data available.

4.4. Additional considerations

Although the primary focus of this study was the technical optimization of solar chimney design for maximum power output, it is worthwhile to consider two broader aspects that could enhance the manuscript and the real-world applicability of the findings: economic feasibility and environmental integration.

4.4.1. Economic feasibility

For a solar chimney to be viable at any scale, its performance benefits must justify the costs of construction and maintenance. The optimized configurations identified (e.g., a 30 m chimney with a large collector achieving ∼15 kW) produce a power output in the order of only tens of kilowatts. In comparison to other renewable technologies, this output is modest, given the physical size of the installation. A preliminary economic assessment would weigh the expected energy yield (and thus revenue or energy savings) against the capital investment (materials for the wide collector, tall chimney structure, turbines, land use, etc.). For instance, a 15 kW output under ideal conditions might generate on the order of 40 MWh per year (assuming a capacity factor of about 30% for a diurnal solar-driven system). If the cost to build a 30 m high chimney with a

∼60 m diameter collector runs into several hundreds of thousands of USD, the levelized cost of electricity could be higher than more established technologies (like photovoltaic or wind), unless significant lifespan and low operational costs tilt the balance. Economies of scale are also relevant: larger solar chimney plants (e.g., approaching the 50 kW of Manzanares or the 200 MW proposals) might benefit from lower cost per kW, but they require enormous structures. Thus, including an economic feasibility discussion would clarify whether the optimized designs are practically implementable or if further innovations (e.g., cost reduction in materials, or multi-purpose usage of the structure) are needed for SCPPs to be competitive. A brief cost–benefit analysis, possibly drawing on literature values for construction costs, could strengthen the argument for where and when solar chimneys make sense as an investment.

4.4.2. Environmental integration

One of the attractive features of solar chimney power plants is their low environmental impact during operation-they produce power with no direct emissions and use simple, largely passive components. An optimized solar chimney could be integrated with other environmental or societal functions. For example, the broad collector area can double as a greenhouse or drying facility for agriculture, or as a water desalination unit (using the sun-heated area to distill water)-providing co-benefits beyond electricity. The updraft airflow might also be harnessed for purposes like ventilation or even water extraction from air in arid climates (some designs propose adding cooling towers or condensers to produce fresh water). These hybrid configurations could improve the overall sustainability and utility of the installation, making a stronger case for implementation. Additionally, the solar chimney could be part of a hybrid energy system, complementing photovoltaic panels (which could potentially be installed around the collector periphery) or thermal energy storage that extends operation beyond daylight hours. By discussing environmental integration, the study highlights that optimizing a solar chimney extends beyond power output to its contribution to sustainable development. Particularly, for rural or remote areas with high solar irradiance (like Lambayeque), an optimally designed chimney could provide power, assist in crop drying or water pumping, and generally improve resilience with minimal ecological footprint. This perspective is reinforced by a recent high-rise integration study, in which a 140-m building incorporated a solar chimney using its roof as the collector, achieving power outputs above 33 kW through turbines positioned at both the chimney base and top.[38]

5. Conclusion

By combining CFD simulations with statistical design-of-experiments techniques, this study identified the key parameters governing the performance of a small-scale solar chimney (approximately 30 m height). Among all geometric factors analyzed, increasing the collector-to-chimney AR and adopting a DC consistently produced the strongest performance gains. The optimal configuration attained a power output of approximately 15 kW, the highest among all simulated cases.

This value is notable, given the moderate dimensions of the system: a 15 kW output represents roughly one quarter of the power generated by the historic Manzanares pilot plant (50 kW), despite our chimney being only one-sixth of its height. This comparison underscores that careful geometric optimization—particularly through collector expansion and chimney divergence—can partially offset the limitations associated with reduced scale.

Additional geometric refinements, such as internal baffles, provided only marginal improvements relative to the optimized base design. The inclusion of a turbine reduced pneumatic power by approximately 10–15%, but did not alter the dominant performance trends: systems with larger AR and divergent geometry consistently outperformed all other configurations.

Overall, the results show that well-designed 30 m chimneys can reach outputs on the order of 7–15 kW. This confirms that relatively small SCPP installations can deliver meaningful power when appropriately optimized. A system of this scale may be suitable for community-level applications or as a supplementary renewable source in distributed energy systems.

From a practical standpoint, the design guidelines identified here offer a clear pathway for improving future solar chimney projects without adding significant structural complexity. Future research should focus on prototype construction and experimental validation under real atmospheric conditions. Extending the analysis to include unsteady day–night cycles, variable solar input, wind effects, and detailed techno-economic assessments would further clarify feasibility. Hybrid configurations—such as coupling the chimney with geothermal waste heat[39] or using curved-guide vanes to increase the airflow path[40]—also

represent promising avenues for enhancing performance and broadening applicability.

Acknowledgments

The authors are grateful to the authorities of the Santo Toribio de Mogrovejo Catholic University (USAT), Peru, for providing the tools and computational resources to conduct this research. Special thanks are extended to Dr. Julio Hilario Vargas, Vice-Rector for Research at USAT, for his institutional support throughout the project. The authors also acknowledge the Faculty of Engineering—in particular the School of Mechanical and Electrical Engineering—and its staff for facilitating this study.

Funding

This research was financially supported by the Santo Toribio de Mogrovejo Catholic University (USAT), Peru (005-2025-USAT-RTDO).

Conflict of interest

The authors declare they have no competing interests.

Author contributions

Conceptualization: Alberto Hananel
Formal analysis: Rodolfo Garcia
Investigation: All authors
Methodology: Alberto Hananel
Writing–original draft: Alberto Hananel
Writing–review & editing: Alberto Hananel, Rodolfo Garcia

Availability of data

The datasets generated and analyzed during the current study are available from the corresponding author on reasonable request.

AI tools statement

The authors confirm that no artificial intelligence (AI) tools were used in the preparation of this manuscript, except for the use of DeepL Pro exclusively for language translation purposes.

References

1. Patel SK, Prasad D, Ahmed, MR. Computational studies on the effect of geometric parameters on the performance of a solar chimney power plant. *Energy Convers Manag.* 2014;77:424–431. https://doi.org/10.1016/j.enconman.2013.09.056
2. Torkfar A, Arefian A, Hosseini-Abardeh R, Bahrami M. Implementation of active and passive control strategies for power generation in a solar chimney power plant: a technical evaluation of Manzanares prototype. *Renewable Energy.* 2023;216:118912. https://doi.org/10.1016/j.renene.2023.118912
3. Rezaei L, Saeidi S, Sápi A, et al. Efficiency improvement of the solar chimneys by insertion of hanging metallic tubes in the collector: experiment and computational fluid dynamics simulation. *J Clean Prod.* 2023;415:137692. https://doi.org/10.1016/j.jclepro.2023.137692
4. Fallah SH, Valipour MS. Numerical investigation of a small scale sloped solar chimney power plant. *Renewable Energy.* 2022;183:1–11. https://doi.org/10.1016/j.renene.2021.10.081
5. Nizetić S. Ninic N, Klarin B. Analysis and feasibility of implementing solar chimney power plants in the Mediterranean region. *Energy.* 2008;33(11):1680–1690. https://doi.org/10.1016/j.energy.2008.05.012
6. , Kassaei F, Bagherzadeh A, Abedi M, Bénard A. Experimental Studies of Solar Chimneys: a Survey of performance, design, and applications for power generation. *Energies.* 2025;18(17). https://doi.org/10.1002/ep.11743
7. Haaf W, Friedrich K, Mayr G, Schlaich J. Solar chimneys part I: Principle and construction of the pilot plant in Manzanares. *Int J Solar Energy.* 1983;2(1):3–20. http://dx.doi.org/10.1080/01425918308909911
8. Haaf W. Solar chimneys part II: Preliminary test results from the Manzanares pilot plant. *Int J Sustain Energy.* 1984;2(2):141–161. https://doi.org/10.1080/01425918408909921
9. Cuce E, Cuce PM, Sen H. A thorough performance assessment of solar chimney power plants: Case study for Manzanares. *Clean Eng Technol.* 2020;1:100026. https://doi.org/10.1016/j.clet.2020.100026
10. Abdelmohimen MAH, Algarni SA. Numerical investigation of solar chimney power plants performance for Saudi Arabia weather conditions. *Sustain Cities Soc.* 2018;38:1–8. https://doi.org/10.1016/j.scs.2017.12.013
11. Li W, Wei P, Zhou X. A cost–benefit analysis of power generation from commercial reinforced concrete solar chimney power plant. *Energy Convers Manag.* 2014;79:104–113. https://doi.org/10.1016/j.enconman.2013.11.046
12. Fasel HF, Meng F, Shams E, Gross A. CFD analysis for solar chimney power plants. *Solar Energy.* 2013;98:12–22. https://doi.org/10.1016/j.solener.2013.08.029
13. Guo P-h, Li J-y, Wang Y. Numerical simulations of solar chimney power plant with radiation model. *Renewable Energy.* 2014;62:24–30. https://doi.org/10.1016/j.renene.2013.06.039
14. Murena F, Gaggiano I, Mele B. Fluid dynamic performances of a solar chimney

plant: Analysis of experimental data and CFD modelling. *Energy*. 2022;249:123702. https://doi.org/10.1016/j.energy.2022.123702
15. Ming T, Liu W, Xu G. Analytical and numerical investigation of the solar chimney power plant systems. *Int J Energy Res*. 2006;30(11):861–873. https://doi.org/10.1002/er.1191
16. Hu S, Leung DYC, Chan JCY. Numerical modelling and comparison of the performance of diffuser-type solar chimneys for power generation. *Appl Energy*. 2017;204:948–957. https://doi.org/10.1016/j.apenergy.2017.03.040
17. Xu Y, Zhou X. Performance of divergent-chimney solar power plants. *Solar Energy*. 2018;170:379–387. https://doi.org/10.1016/j.solener.2018.05.068
18. Nasraoui H, Driss Z, Kchaou H. Effect of the chimney design on the thermal characteristics in solar chimney power plant. *J Therm Anal Calorim*. 2020;140:2721–2732. https://doi.org/10.1007/s10973-019-09037-3
19. Singh T, Kumar A. Numerical analysis of the divergent solar chimney power plant with a novel arc and fillet radius at the chimney base region. *Renewable Energy*. 2024;228:120504. https://doi.org/10.1016/j.renene.2024.120504
20. Vieira RS, Petry AP, Rocha LAO, Isoldi LA, Dos Santos ED. Numerical evaluation of a solar chimney geometry for different ground temperatures by means of constructal design. *Renewable Energy*. 2017;109:222–234. https://doi.org/10.1016/j.renene.2017.03.007
21. Arzpeyma M, Mekhilef S, Newaz KMS, et al. Solar chimney power plant and its correlation with ambient wind effect. *J Therm Anal Calorim*. 2020;141(2):649–668. https://doi.org/10.1007/s10973-019-09065-z
22. Bagheri S, Hassanabad MG. Numerical and experimental investigation of a novel vertical solar chimney power plant for renewable energy production in urban areas. *Sustain Cities Soc*. 2023;96:104700. https://doi.org/10.1016/j.scs.2023.104700
23. Mebarki A, Sekhri A, Assassi A, Hanafi A, Marir B. CFD analysis of solar chimney power plant: Finding a relationship between model minimization and its performance for use in urban areas. *Energy Reports*. 2022;8:500–513. https://doi.org/10.1016/j.egyr.2021.12.008
24. Canada G. RETScreen® Clean Energy Management Software. https://natural-resources.canada.ca/maps-tools-and-publications/tools/modelling-tools/retscreen/7465
25. Group WB, Denmark (DTU) TU. Global Solar Atlas. https://globalwindatlas.info/es
26. Sharon H. A detailed review on sole and hybrid solar chimney based sustainable ventilation, power generation, and potable water production systems. *En Nex*. 2023;10:100184. https://doi.org/10.1016/j.nexus.2023.100184
27. Behera BK, Sahoo SS, Kumar S. Technology, design, and performance of solar chimney power plants: An updated and thorough review. *Int J Renew Energy Res*. 2024;22(9):1816-1849 (Published online 28 Dec 2024). https://doi.org/10.1080/15435075.2024.2446492
28. Mandal DK, Gupta KK, Biswas N, Manna NK, Santra S, Benim AC. Optimization of hybrid solar chimney power plants (HSCPPs): A review of multi-objective approaches. *Applied Energy*. 2025;396:126214. https://doi.org/10.1016/j.apenergy.2025.126214
29. Hachicha AA, Abo-Zahhad EM, Masmoudi M, Said Z, Rahman S. Techno-Economic evaluation and multi-objective optimization of a filter equipped solar chimney system. *Renewable Energy*. 2024;237:121452. https://doi.org/10.1016/j.renene.2024.121452
30. Ferziger JH, Perić M. Computational Methods for Fluid Dynamics. Berlin, Heidelberg: Springer- Verlag Berlin Heidelberg3 ed. 2002. https://doi.org/10.1007/978-3-642-56026-2
31. Kröger DG, Blaine D. Analysis of the driving potential of a solar chimney power plant. *J R&D* . 1999;15:85–94. Accessed 16 Oct. 2025.
32. POWER NASA Project. The Prediction of Worldwide Energy Resource (POWER); 2024. https://power.larc.nasa.gov/. NASA Applied Sciences Program within the Earth Science Division of the Science Mission Directorate.
33. Montgomery D. Design and analysis of experiments, 8th edition. *Environ Prog Sustain Energy*. 2013;32(1):8-10. https://doi.org/10.1002/ep.11743
34. Rahim M, Amin F, Shah K, Ahmad T. Some distance measures for Pythagorean cubic fuzzy sets: Application selection in optimal treatment for depression and anxiety. *MethodsX*. 2024;12:102678. https://doi.org/10.1016/j.mex.2023.102678
35. Khan S, Shah K, Debbouche A, Zeb S, Antonov V. Solvability and Ulam-Hyers stability analysis for nonlinear piecewise fractional cancer dynamic systems. *Phys Scr*. 2024;99(2):025225. https://doi.org/10.1088/1402-4896/ace526
36. Aldwoah K, Almalahi MA, Hleili M, Alqarni FA, Aly ES, Shah K. Analytical study of a modified-ABC fractional order breast cancer model. *J Comput Appl Math*. 2024;70(4):3685-3716. https://doi.org/10.1007/s12190-024-02102-7
37. Bakri B, Benguesmia H, Nasraoui H, Driss Z. Experimental study of solar chimney power plant under the climatic conditions of Sfax, Tunisia. *J Adv Res Fluid Mech Therm Sci*. 2023;101(1):207-214. https://doi.org/10.37934/arfmts.101.1.207214
38. Titi MH, Mebarki A, Assassi A. Integration of the Manzanares solar chimney power plants in towers: Collector and building height configuration. *Eng Technol Appl Sci Res*. 2025;15(3):23002-23007. https://doi.org/10.48084/etasr.10594

39. Tesfa TG, Alemu AG. Integrating geothermal waste heat into solar chimney power plant design for improved performance. In *Int J Green Energy* (Springer). 2025;211-236. https://doi.org/10.1007/978-3-031-81730-4$_1$2
40. Elsayed AM, Gaheen OA, Aziz MA. Enhancing solar chimney power plant performance through innovative collector curved-guide vanes configurations. *Renewable Energy.* 2024;232:121127. https://doi.org/10.1016/j.renene.2023.121127

Alberto Hananel *is a Peruvian mathematician (PhD, International Doctorate, University of Granada; Fundación Carolina scholar) and full-time faculty at Universidad Católica Santo Toribio de Mogrovejo (USAT), Peru. He also holds a Second Specialisation Degree in Engineering in Applied Statistics for Research. His work integrates finite element methods, numerical analysis of differential equations, multivariate statistics, computational fluid dynamics (CFD) and AI-assisted modelling. He has led multiple funded projects as principal investigator, including the award-winning programme ''Optimisation of Solar Chimney Design through CFD Simulations and Multivariate Analysis with Chernoff Faces". His publications span Scopus and Web of Science journals, books and conference proceedings. As corresponding author, he focuses on computational and optimisation approaches with direct engineering impact, particularly in renewable energy and advanced modelling for decision-making.*
https://orcid.org/0000-0003-4113-8623

Rodolfo Garcia *is a Professor at the Faculty of Engineering and Architecture of Universidad Católica Santo Toribio de Mogrovejo (USAT), Peru, where he conducts research in Computational Fluid Dynamics (CFD) and its applications to renewable energy and thermal systems. He holds a Master's degree in Advanced Mechanical Engineering from the University of Warwick, United Kingdom, supported by the "Beca Generación del Bicentenario" scholarship awarded by the Peruvian Government. His academic and professional experience focuses on CFD modelling, heat transfer optimisation, and the numerical analysis of fluid–structure interaction. He has participated in multidisciplinary projects involving solar energy systems, industrial process optimisation, and sustainable design. His research seeks to bridge theory and practice by advancing computational techniques that improve engineering performance and energy efficiency. He collaborates with national and international institutions to promote applied research and innovation in computational and energy engineering.*
https://orcid.org/0000-0002-9541-6257

Alejandro Vera *has a Doctor in Science and Engineering, specialised in Mechanical Vibrations using wavelet and Hilbert-Huang Transform (HHT) analysis. He also holds a Master's degree in Mechanical and Electrical Engineering (Energy major, UNPRG–CARELEC) and a Bachelor's degree in Mechanical Engineering (UNT, Peru). His academic background includes diplomas in Computer-Aided Design and Engineering (CAD-CAE), specialising in finite element analysis of machines and structures, and in Industrial Maintenance Management. He specialises in energy efficiency, energy planning for industrial and mining sectors, ISO 50001 implementation, and vibrational analysis of rotating machinery. He works as an independent consultant in reliability engineering, applying predictive techniques with Matlab and Power BI, and has contributed to the digitalisation and energy transition of hydroelectric power plants. At Universidad Católica Santo Toribio de Mogrovejo (USAT), Peru, he conducts research and lectures in mechanical design, reliability engineering, energy systems, and asset management.*
https://orcid.org/0000-0003-0198-338X

Appendix

Table A1. Comparative summary: Optimal combinations, maximum power, key factors, and relevant observations based on computational fluid dynamics results

Design	Optimal combination	Max. power (kW)	Key factors	Relevant observations
RCBD	(i) AR = 6 (ii) Divergent chimney	∼16	(i) AR (ii) chimney type	Higher AR significantly improves power output; the divergent chimney adds a further increase. Low AR notably reduces performance (7–10 kW).
Two-factor ANOVA	(i) AR = 6 (ii) Region 2	∼12	(i) AR (ii) region	AR = 6 outperformed AR = 2 in all regions; Region 2 (warm climate) produced the highest power. No significant AR–region interaction (AR effect consistent across climates).
ANOVA-3	(i) AR = 6 (ii) Divergent chimney (iii) No turbine	∼15	(i) AR (ii) chimney type turbine	High AR and divergent chimney maximize power. The turbine reduces power by ∼15% (from 15 to 13 kW) but does not alter the ranking of effects; no significant factor interactions were detected.
LSD	(i) AR = 6 (ii) H = 30 m (iii) Divergent chimney	∼15	(i) AR (i) chimney type (height)	Statistically confirmed that AR and chimney geometry are the most influential factors; with low AR, power drops to ∼8–10 kW. Confirms trends observed in factorial designs.
GLSD	(i) AR = 6 (ii) H = 30 m (iii) Divergent chimney (iv) Concrete material	∼16	(i) AR (ii) chimney type (material)	AR and divergent chimney dominate performance; high-inertia material (concrete) provided a secondary improvement. With lighter materials or lower AR, power decreased (∼11–13 kW).
FrF_2-N	(i) AR = 6 (ii) Divergent chimney (iii) No neck	∼14	(i) AR (ii) chimney type (neck n.s.)	High AR and divergent chimney increased power, while inclusion of a "neck" had no significant effect. Max. power ∼14 kW, consistent with values from equivalent full designs.
BIBD	(i) AR = 6 (ii) Divergent chimney	∼15	(i) AR (ii) chimney type	Even with incomplete combinations, the divergent chimney yielded the highest power (∼15 kW, followed by Co ∼12 kW). Configurations with AR = 2–4 only achieved ∼9–10 kW. Confirms the superiority of a wide collector and divergent tower even under partial sampling.
GLM	(i) AR = 6 (ii) Divergent chimney	∼14	(i) AR (ii) chimney type (others)	The metamodel confirmed that AR and chimney divergence are dominant factors (others have minor effects). Predicted max. power of ∼14 kW for high AR with divergent chimney, matching observed trends; enabled interpolation of unsimulated configurations, validating conclusions.
Nested	(i) AR = 6 (ii) Divergent chimney	∼16	(i) AR (ii) chimney type	The nested design showed that even within a given AR, geometric variations (DC vs. CC) significantly influence performance. AR = 6 with divergent chimney reached ∼16 kW. Trend consistency confirmed even when examining intra-AR variation.
Split-Plot	(i) AR = 6 (ii) Divergent chimney	∼18	(i) AR (ii) chimney type	Under varying environmental conditions, high AR and divergent chimney reached ∼18 kW, while AR = 2 with cylindrical chimney only ∼8–9 kW. Patterns remained stable across conditions (irradiance and temperature affect magnitude but not design ranking).
Unbalanced	(i) AR = 6 (ii) Divergent chimney	∼14	(i) AR (ii) chimney type	Unbalanced analysis again identified AR = 6 with divergent chimney as optimal (∼14 kW; second best: AR = 6 with Co, 11–12 kW). AR = 2–4 configurations delivered only ∼7–10 kW. Even with irregular data, a high AR and divergent tower remain key performance drivers.